Stormier Southern Hemisphere induced by topography and ocean circulation

Tiffany A. Shaw[a,1], **Osamu Miyawaki**[a], **and Aaron Donohoe**[b]

[a]Department of the Geophysical Sciences, The University of Chicago, Chicago, IL, 60637; [b]Applied Physics Laboratory, University of Washington, Seattle, WA, 98105

This manuscript was compiled on April 11, 2022

A defining feature of Earth's present-day climate is that the Southern Hemisphere is stormier than the Northern Hemisphere. Consistently, the Southern Hemisphere has a stronger jet stream and more extreme weather events than the Northern Hemisphere. Understanding the relative importance of land-ocean contrast, including topography, radiative processes and ocean circulation for determining this storminess asymmetry is important and may be helpful for interpreting projections of future storminess. Here we show the stormier Southern Hemisphere is caused by nearly equal contributions from topography and the ocean circulation, which moves energy from the Southern to Northern Hemisphere. These findings are based on 1) diagnostic energetic analyses applied to observations and climate model simulations and 2) modifying surface (land and ocean) boundary conditions in climate model simulations. Flattening topography and prescribing hemispherically symmetric surface energy fluxes (the manifestation of ocean energy transport on the atmosphere) in a climate model reduces the storminess asymmetry from 23% to 12% and 11%, respectively. Finally, we use the energetic perspective to interpret storminess trends since the beginning of the satellite era. We show the Southern Hemisphere has become stormier, consistent with implied ocean energy transport changes in the Southern Ocean and climate model projections. In the Northern Hemisphere storminess has not changed significantly consistent with oceanic and radiative (increased absorption of sunlight due to the loss of sea ice and snow) changes opposing one another. The storminess trends are projected to continue throughout the 21st century.

extratropical storms | ocean circulation | climate change

A defining feature of Earth's present-day climate is that extratropical storminess in the Southern Hemisphere is stronger than its Northern Hemisphere counterpart (1–4). The jet stream is also stronger in the Southern Hemisphere (5). These differences are important because they result in more precipitation and wind extremes across the extratropical Southern Hemisphere (6, 7). The relative roles of land-ocean contrast, including topography, radiative processes and ocean circulation in determining this storminess asymmetry is unknown. Uncovering the mechanisms controlling present-day storminess is an important step toward understanding future projections of storminess, including their societal impacts (4, 8).

Present-day storminess in the Southern Hemisphere is distributed nearly homogeneously across the Southern Ocean (Fig. 1a). In contrast, Northern Hemisphere storminess is localized mostly over ocean basins (Fig. 1b). The storminess asymmetry (Southern minus Northern Hemisphere) reflects land and ocean boundary conditions in the Northern Hemisphere (Fig. 1c). More specifically, the longitudinal regions where the Southern Hemisphere is stormier (orange contours, Fig. 1c) coincide with regions of large topography over Eurasia and North America. When averaged over longitude and across the extratropics (poleward of 20° latitude) the Southern Hemisphere is ∼24% stormier than the Northern Hemisphere across reanalysis data sets (Fig. S1a). The storminess asymmetry is largest in the upper troposphere and is also clear in the jet stream (Fig. S1b,c).

The observed storminess asymmetry can be simulated in an atmospheric model forced with topography and observationally-derived surface energy fluxes (the manifestation of ocean energy transport on the atmosphere). The model captures both the spatial structure (c.f. Fig. 1c and Fig. 2a) and the extratropical storminess asymmetry, which is ∼23% in the model compared to ∼24% in observations (c.f. Fig. S1a and Fig. 2e, Table 1).

Topographic contribution to present-day storminess

Results from early climate model simulations showed flattening topography significantly increases storminess in the Northern Hemisphere (9). However, the modeled storminess did not capture the observed storminess asymmetry. In particular, the Southern Hemisphere storminess was biased. Here we show flattening topography in the model which captures the observed storminess asymmetry reduces but does not eliminate the asymmetry (Fig. 2b). Storminess increases in both hemispheres when topography is flattened (Table 1 FLAT) but Southern Hemisphere storminess is still stronger than Northern Hemisphere storminess across the Eastern Hemisphere

Significance Statement

Storms and extreme weather events are stronger in the Southern Hemisphere than in the Northern Hemisphere. Using an energetic perspective, observations and climate model simulations we show that this defining feature of Earth's present-day climate is caused by nearly equal contributions from topography and the ocean circulation, which transports energy from the Southern to the Northern Hemisphere. We also show the recent increase in Southern Hemisphere storminess is connected to changes in implied ocean energy transport in the Southern Ocean. Northern Hemisphere storminess has not changed significantly because the ocean changes are opposed by the absorption of sunlight due to the loss of sea ice and snow. These observed changes are broadly consistent with climate model projections.

T.A.S. formulated the energetic mechanism, designed and performed the climate model simulations. O. M. and A. D. downloaded the reanalysis and CMIP5 model data. All authors contributed to the writing of the manuscript.

The authors declare no conflict of interest.

[1]To whom correspondence should be addressed. E-mail: tas1@uchicago.edu

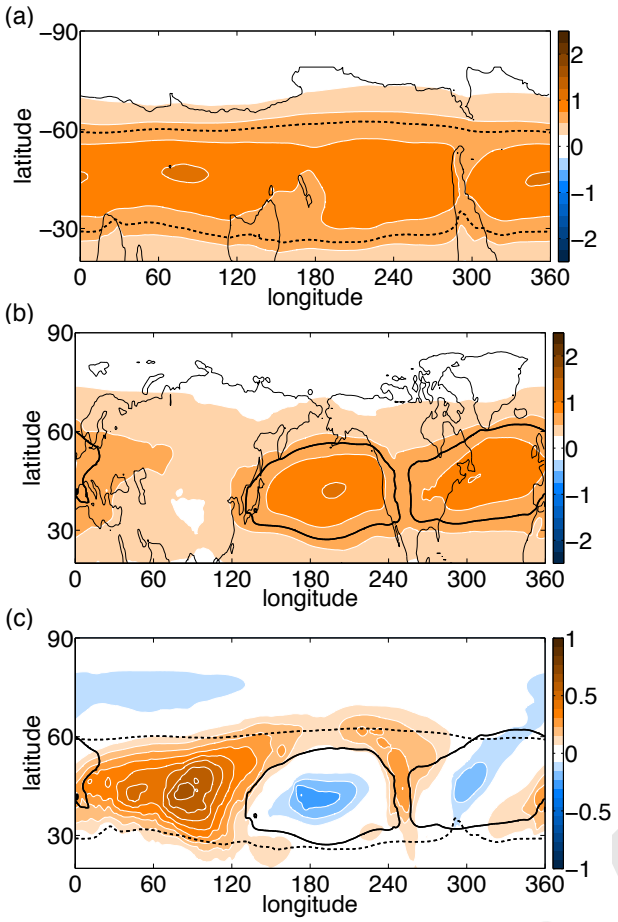

Fig. 1. Observed annual-mean storminess (averaged across reanalysis data sets) as measured by vertically-integrated eddy kinetic energy (MJm^{-2}) from 1980 to 2018 for the (a) Southern Hemisphere, (b) Northern Hemisphere and (c) their difference. The black lines indicate where storminess is equal to 0.6 MJm^{-2} for the Southern (dashed) and Northern (solid) hemispheres.

and between 30° to 45° latitude in the Western Hemisphere (Fig. 2b). When averaged over longitude and across the extratropics the storminess asymmetry is reduced from ∼23% to ∼12% with flattened topography (Fig. 2e FLAT), which is large compared to projections of the response of storminess to anthropogenic climate change at the end of the 21st century (10).

An existing framework based on temperature (10, 11) cannot explain the reduced storminess asymmetry when topography is flattened (MAPE asymmetry is ∼23% for ALL and FLAT, Table 1). Instead we turn to an energetic framework, which connects extratropical storminess (STM) to three factors: the equator-to-pole imbalance of top-of-atmosphere radiative fluxes (TOA), the equator-to-pole imbalance of surface energy fluxes (SFC) and stationary circulation atmospheric energy flux (SC):

$$STM = TOA - SFC - SC \quad [1]$$

(Methods, 12). Topography influences storminess through the stationary circulation atmospheric energy flux (13, 14).

In observations, the energetic storminess asymmetry (STM) is ∼23% and can be diagnostically decomposed into a 12% contribution from surface energy fluxes (-SFC), a ∼14% contribution from stationary circulation atmospheric energy flux (-SC) and a small ∼-3% contribution from TOA radiative fluxes (Fig. S2). The small TOA contribution is consistent with the small hemispheric asymmetry of TOA radiative fluxes (15–17).

Table 1. Storminess (vertically-integrated eddy kinetic energy, EKE, MJm^{-2}) and moist Mean Available Potential Energy (MAPE, MJm^{-2}) calculated following (10) and averaged across the extratropics (averaged poleward of 20°) of the Northern (NH) and Southern (SH) Hemispheres.

	EKE_{NH}	EKE_{SH}	$MAPE_{NH}$	$MAPE_{SH}$
ALL	0.82	1.00	3.02	3.73
FLAT	0.95	1.06	3.04	3.76
SYMS	0.84	0.93	3.05	3.67
F + S	0.96	1.00	3.08	3.61

When the model is forced with topography and observationally-derived surface energy fluxes, it captures the diagnostic decomposition of the storminess asymmetry in observations, namely a 12% contribution from surface energy fluxes (-SFC), a ∼14% contribution from stationary circulation atmospheric energy flux (-SC) and a small ∼-3% contribution from TOA radiative fluxes (Fig. 2f ALL).

When topography is flattened in the model, the stationary circulation contribution to the storminess asymmetry becomes negligible (consistent with its connection to topography) and the remaining asymmetry is due to surface energy fluxes (Fig. 2f FLAT). Thus, the model simulation with flattened topography confirms the causal connection between the stationary circulation contribution and topography and shows topography accounts for about half of the storminess asymmetry.

Oceanic contribution to present-day storminess

Another important source of hemispheric asymmetry is the ocean circulation. The ocean transports energy poleward in both hemispheres but also across the equator from the Southern to the Northern Hemisphere via the ocean overturning circulation (18). The ocean overturning circulation is known to modulate the wintertime climate of the Northern Hemisphere, including the intensity of storminess in the North Atlantic (19–23). Frierson et al. (16) showed the ocean overturning circulation contributes to the hemispheric asymmetry of tropical precipitation. However, the impact of the ocean circulation on the storminess asymmetry has not been previously examined.

Here we hypothesize the ocean makes the present-day Southern Hemisphere stormier than the Northern Hemisphere via the following energetic mechanism. The ocean overturning circulation transports energy from the Southern to the Northern Hemisphere converging energy into the Arctic. The hemispheric asymmetry of ocean energy transport manifests onto the atmospheric energy budget as a hemispheric asymmetry of surface energy fluxes (16) (provided the land and ocean surface is in equilibrium). Thus, due to ocean circulation alone the Southern Hemisphere should be stormier than the Northern Hemisphere because it leads to a weaker equator-to-pole imbalance of surface energy fluxes in the North. The impact of the ocean circulation on the hemispheric asymmetry of storminess is reflected in the SFC contribution of the energetic framework (equation 1). Note this mechanism suggests that if the hemispheric asymmetry of surface energy fluxes were

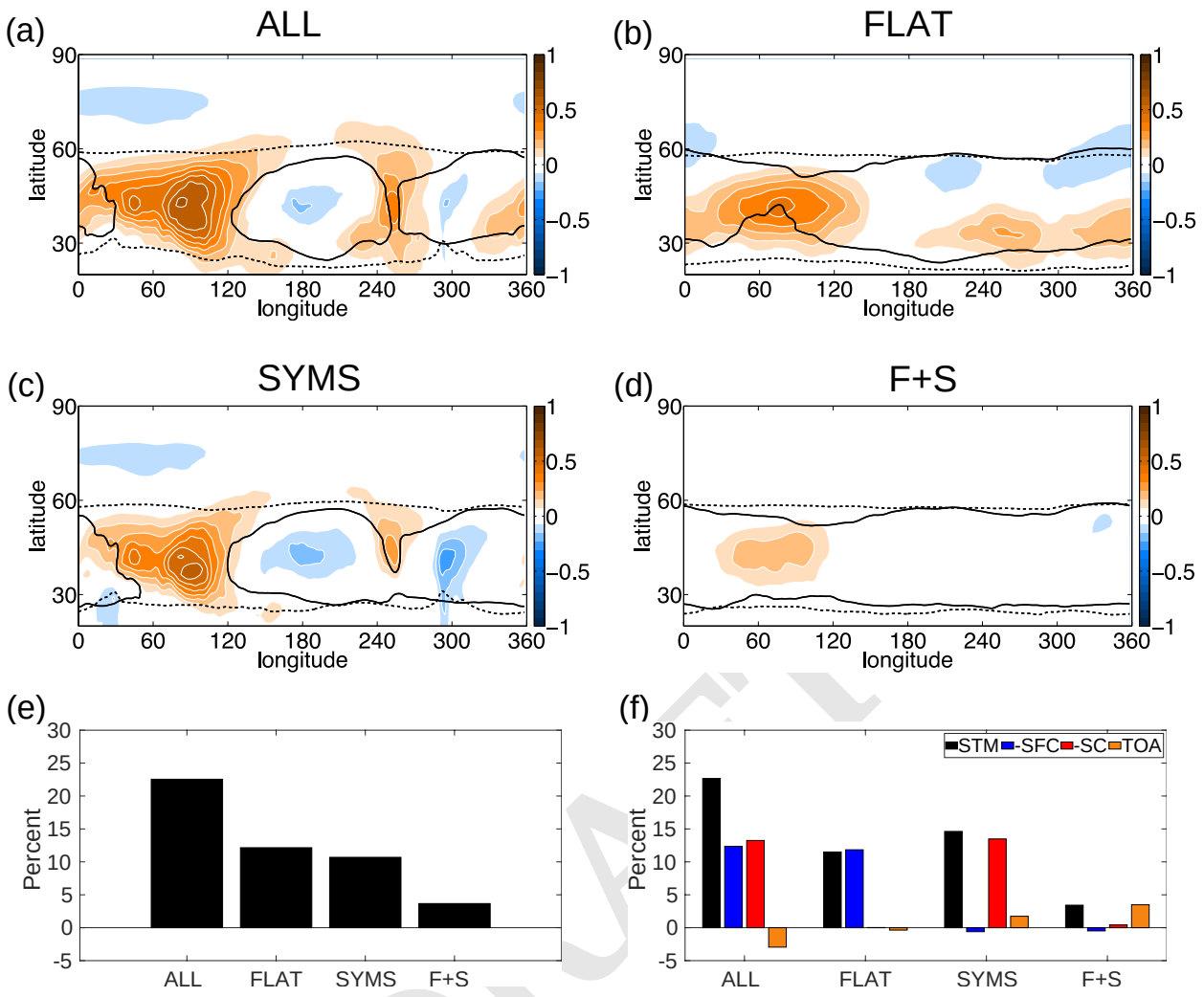

Fig. 2. Difference of Southern and Northern Hemisphere storminess (vertically-integrated eddy kinetic energy, MJm^{-2}) in the climate model simulation for (a) climatology (ALL), (b) flattened topography (FLAT), (c) symmetrized surface energy fluxes (SYMS), and (d) flattened topography and symmetrized surface energy fluxes (F+S) simulations. The black lines in (a)-(d) indicate where storminess is equal to 0.6 MJm^{-2} for the Southern (dashed) and Northern (solid) hemispheres. Percentage difference of longitudinal-mean, vertically-integrated extratropical (poleward of 20°) storminess (difference of Southern and Northern Hemisphere divided by Northern Hemisphere) across the simulations for (e) eddy kinetic energy and (f) transient eddy moist static energy flux (STM) decomposed into surface energy flux (SFC), stationary circulation (SC) and top-of-atmosphere (TOA) contributions.

eliminated then the storminess asymmetry would be reduced.

We analyze the impact of the ocean circulation on the storminess asymmetry by forcing the climate model with hemispherically symmetrized surface energy fluxes following Frierson et al. (16). Recall when the climate model is forced with observationally-derived surface energy fluxes it captures the storminess asymmetry, namely the Southern Hemisphere is stormier than the Northern Hemisphere (Fig. 2a and Fig. 2e ALL). When the model is forced with hemispherically symmetrized surface energy fluxes, which eliminates the hemispheric asymmetry of ocean energy transport (Fig. S3), the storminess asymmetry decreases (Fig. 2c). The decreased asymmetry occurs because Northern Hemisphere storminess increases whereas Southern Hemisphere storminess decreases (Table 1 SYMS). The impact of symmetrizing surface energy fluxes on storminess is more longitudinally homogeneous than the impact of flattening topography (compare Fig. 2b to 2c). However, the storminess asymmetry is still significant over the Eastern Hemisphere and between 45° to 60° latitude in the Western Hemisphere. We interpret this result as the combined impact of topography and land boundary conditions on storminess. When averaged over longitude and across the extratropics the storminess asymmetry is reduced from ∼23% to ∼11% with symmetrized surface energy fluxes (Fig. 2e SYMS).

In order to confirm the causal role of the ocean circulation we turn to the energetic framework. When surface energy fluxes are hemispherically symmetrized in the model, the surface energy flux contribution to the storminess asymmetry becomes negligible (consistent with its connection to the hemispheric asymmetry of implied ocean energy transport) and the remaining asymmetry is due to the stationary circulation energy flux (Fig. 2f SYMS). Thus, the model simulation with hemispherically symmetrized surface energy fluxes confirms the ocean circulation accounts for about half of the storminess asymmetry.

When the model is forced with hemispherically symmetrized surface energy fluxes in the presence of flattened topography

the storminess asymmetry is negligible (Fig. 2d), i.e. ∼3% (Fig. 2e F+S). In particular, Northern Hemisphere storminess is now similar to Southern Hemisphere storminess (Table 1 F+S). The jet stream asymmetry is also negligible (Fig. S4). When topography is flattened in the presence of hemispherically symmetrized surface energy fluxes in the model, the stationary circulation and surface energy flux contributions are negligible. The TOA radiative flux contribution leads to a small storminess asymmetry (Fig. 2f F+S).

Thus, the present-day storminess asymmetry is caused by nearly equal contributions from topography and the ocean circulation. Interestingly, the results imply that differences in evaporative resistance over land, land-ocean surface heat capacity, or surface drag do not contribute significantly to the stormier Southern Hemisphere.

Contributions to the strengthening of Southern Hemisphere storminess

Since the beginning of the satellite era, the Southern Hemisphere has become even stormier than the Northern Hemisphere, consistent with climate model projections (Fig. 3a). This trend reflects a significant strengthening of Southern Hemisphere storminess and no significant change in Northern Hemisphere storminess (Table S1).

The energetic perspective can be used to interpret why the Southern Hemisphere is getting stormier. According to the energetic framework, the increasingly stormier Southern Hemisphere (black bar, Fig. 3b) is consistent with the surface energy flux trend (blue bar, Fig. 3b). The surface energy flux trend reflects anomalous equatorward implied ocean energy transport, which is stronger in the Southern Ocean than in the North Atlantic (blue line, Fig. S5a). The anomalous implied equatorward transport in the Southern Ocean has been connected to circumpolar upwelling and passive advection by the climatological ocean circulation associated with the transient response to increased CO_2 (24). We note that our analysis cannot distinguish between trends in ocean energy transport and the spatial pattern of ocean energy content and we use the term “implied" to refer to both processes.

Another important factor contributing to the increasingly stormier Southern Hemisphere is the TOA radiative flux trend (orange bar, Fig. 3b). The hemispheric asymmetry of TOA radiative flux trend reflects increased absorption of sunlight in the Northern Hemisphere which is unmatched in the Southern Hemisphere (Fig. S6). Arctic sea ice loss (25) and snow melt over the Northern Hemisphere continents (26) are consistent with enhanced absorption of shortwave radiation in the NH extratropics, which weakens the TOA contribution to Northern Hemisphere storminess (Fig. S5) and, thus, results in a positive storminess asymmetry trend (orange bar, Fig. 3b). The hemispheric asymmetry of TOA radiative flux trend is consistent with the transient climate response to increased CO_2, which differs between the hemispheres. In climate models the transient response to increased CO_2 involves Arctic Sea ice loss, Arctic amplification of surface temperature, snow melt over Northern Hemisphere continents, and land warming more than ocean. In contrast the transient response involves negligible changes in Antarctic Sea ice and no Antarctic amplification of surface temperature. Instead, transient cooling occurs over the Southern Ocean (27, 28). Consistently climate models simulate a larger hemispheric asymmetry of radiative changes for the transient response than the quasi-equilibrium response, which involves Antarctic Sea ice loss and Antarctic amplification of surface temperature (28, 29).

The radiative and surface energy flux trends are opposed by the stationary circulation energy flux trend (red bar, Fig. 3b). The stationary circulation trend reflects an increase in the Southern hemisphere stationary circulation energy flux from 20-40S and small changes in the Northern Hemisphere (Fig. S5). The Southern Hemisphere stationary circulation trend is dominated by the mean meridional circulation (Hadley and Ferrel cell) contribution (Fig. S7). The connection between documented trends in the Hadley cell (30) and the stationary circulation energy flux is currently unclear. Our diagnostic analysis also cannot rule out the possibility that the stationary circulation energy flux trend is related to the surface energy flux trend.

The trends in climate model projections are consistent in sign with reanalysis data but climate models underestimate the magnitude (Fig. 3c). The models also do not fully capture the spatial structure of the changes (Fig. S5b). According to the model projections, the Southern Hemisphere will continue to get stormier throughout the 21st century (Table S1).

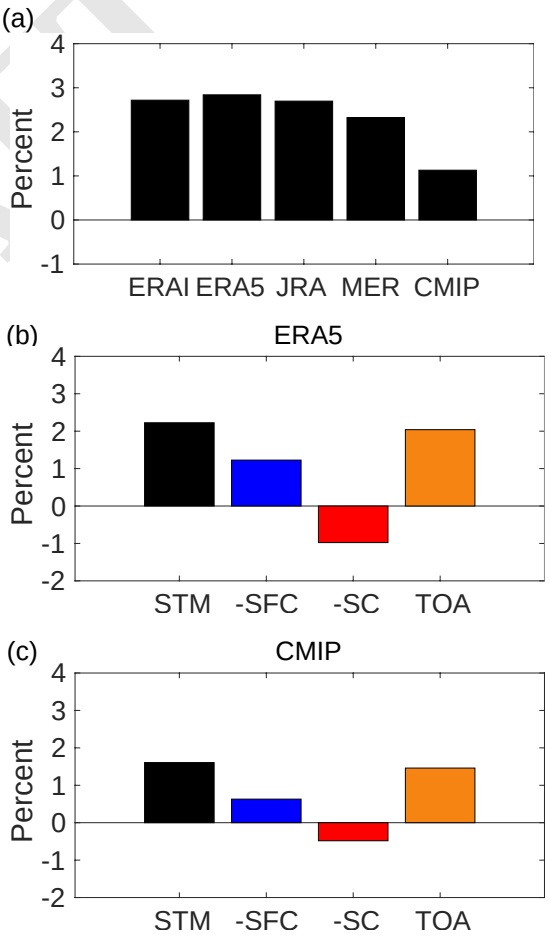

Fig. 3. Trend of storminess asymmetry (difference of Southern and Northern Hemisphere divided by Northern Hemisphere climatology) from 1980 to 2018 in reanalysis data and CMIP5 models as measured by vertically-integrated (a) eddy kinetic energy and eddy moist static energy flux (STM) decomposed into surface energy flux (SFC), stationary circulation energy flux (SC) and TOA radiative flux (TOA) contributions in (b) ERA5 and (c) CMIP5 data. All trends are multiplied by 39 years.

Discussion

Our results show the Southern Hemisphere is stormier than the Northern Hemisphere because of topography and the ocean circulation. We showed the impact of topography and the ocean circulation could be interpreted using an energetic framework that linked topography to the stationary circulation atmospheric energy flux and the ocean circulation to surface energy fluxes. More specifically, the ocean circulation contributes to a stormier Southern Hemisphere by transporting energy from the Southern to the Northern Hemisphere thereby creating a larger equator-to-pole surface energy flux imbalance in the Southern Hemisphere. The causal impact of topography and ocean circulation was confirmed by combining 1) diagnostic energetic analysis of observations and climate model simulations and 2) climate model simulations with modified (land and ocean) surface boundary conditions (flattened topography and hemispherically symmetrized surface energy fluxes). Interestingly, the results show land-ocean contrast (surface heat capacity, evaporative resistance over land, and surface drag) alone does not result in a stormier Southern Hemisphere.

The energetic perspective of storminess was used to interpret why the Southern Hemisphere has become stormier since the beginning of the satellite era. In particular, the stormier Southern Hemisphere is consistent with anomalous equatorward implied ocean energy transport in the Southern Ocean. In the Northern Hemisphere, TOA radiative changes associated with the loss of sea ice and snow oppose the strengthening of storminess implied from ocean changes. These observed trends are broadly consistent with climate model projections of the transient climate response to increased CO_2. Namely, the Southern Hemisphere is projected to become stormier in the future whereas Northern Hemisphere storminess changes will be muted due to a tug of war between tropical and polar climate changes (4, 31).

Our energetic mechanism accounts for thermodynamic coupling between the atmosphere and ocean. It does not preclude the impact of dynamic coupling. Indeed dynamic coupling between the atmosphere and ocean could contribute to the storminess asymmetry if it significantly impacts surface energy fluxes. A recent study (32) showed that flattening topography in coupled models leads to a weaker ocean circulation but the impact on storminess is consistent with our atmospheric model results (storminess asymmetry is still significant with flattened topography). The impact of ocean-atmosphere interactions on storminess should be studied further using coupled climate models and observations.

The energetic mechanism linking the ocean circulation to the extratropical storminess asymmetry has implications for our understanding of storminess in past climates. In particular during the Last Glacial Maximum (LGM) the ocean overturning circulation was weaker than present-day, which would tend to weaken the storminess asymmetry following the energetic mechanism (weaker Southern Hemisphere storminess). However, topography was elevated in the Northern Hemisphere during the LGM because of the Laurentide ice sheet, which would tend to strengthen the storminess asymmetry (weaker Northern Hemisphere storminess). There is evidence for weaker North Atlantic storminess (33–35) and small changes in Southern Hemisphere storminess across an ensemble of LGM climate model simulations (36). The energetic framework can be used to further investigate the connections between radiative fluxes, ocean circulation, topography and storminess across different climates.

Materials and Methods

Observational data products. We use 6 hourly data provided by ERA-Interim, ERA5, MERRA2 and JRA-55 from 1980 to 2018. We quantify storminess using the vertically-integrated transient eddy kinetic energy and eddy moist static energy flux. In both cases transient eddies are defined as deviations from a monthly average, that is an average over a particular month not the climatological monthly average (12).

Since surface energy fluxes are not measured directly, we create an observational estimate following previous work (16, 37, 38). In particular, we estimate the climatological surface energy flux by subtracting atmospheric energy flux divergence estimates based on reanalysis data from satellite observations of TOA radiative flux. The Clouds and the Earth's Radiant Energy System (CERES) Energy Balanced and Filled (EBAF) satellite product data from 2001 to 2018 is used to estimate the TOA radiative flux and the atmospheric energy flux divergence is estimated using ERA-Interim from 2001 to 2018. While we use the most accurate method for estimating surface energy fluxes there remains some uncertainty in any energy budget estimate.

Trends in the storminess asymmetry are significant from 1980 to 2018 but not from the 2001 to 2018 period for which satellite derived TOA radiative flux from CERES EBAF is available. In order to understand the storminess trends from 1980 to 2018 and their connection to surface energy fluxes we use the same method to quantify trends of surface energy fluxes. Namely, we take the difference of TOA radiative flux and atmospheric energy flux divergence and storage (accounting for the small atmospheric energy storage). However, we do not trust trends in the surface energy fluxes from the reanalysis output (i.e. the combination of surface radiative and turbulent energy fluxes in the reanalysis) due to well documented unrealistic energy imbalances and drifts (39, 40). Thus, we estimate surface energy fluxes from 1980 to 2018 from the difference of ERA5 TOA radiative flux and the atmospheric energy flux divergence derived from 6 hourly ERA5 reanalysis data. We use the ERA5 TOA radiative flux data because it agrees better with CERES data from 2001 to 2018 as compared to the other reanalysis TOA radiative fluxes (Fig. S8). In all cases trends are calculated using a linear regression model. The vertically-integrated eddy kinetic energy trends are consistent with the 700 hPa eddy heat flux trends in the Southern Hemisphere (41).

Climate model simulations. We simulate storminess using the ECHAM6 slab-ocean atmosphere general circulation model (42). The model has a realistic land surface with topography, a 50 m mixed layer depth and is forced with the surface energy fluxes derived from 1) an observational estimate (see above) and 2) a q-flux from a prescribed sea surface temperature (AMIP) simulation.

Topography is flattened in the ECHAM6 simulations by setting the surface geopotential and mean orography to zero in the surface boundary condition input file. Symmetrized surface energy fluxes are created following the procedure of (16). Namely, the symmetrized surface energy flux is longitudinally symmetric, with values chosen at each latitude such that the longitudinal integral of the surface energy flux over the ocean is equal to the average between the Northern Hemisphere and Southern Hemisphere longitudinal integrals. The storminess simulated using symmetrized surface energy fluxes and flattened topography are robust to using either the observationally-derived or q-flux derived surface energy fluxes (compare Fig. 2 to Fig. S9).

We use daily data from 22 coupled CMIP5 models (Table S2) to calculate storminess from 1980 to 2018 (Historical and RCP8.5) and 2061 to 2099 (RCP8.5).

Energetic Framework. The moist static energy (MSE) framework for storm track intensity connects extratropical storminess to TOA

radiative fluxes, surface energy fluxes and stationary circulation energy fluxes via the MSE budget

$$\nabla \cdot F_{TE} = \nabla \cdot F_{TOA} - \nabla \cdot F_{SFC} - \nabla \cdot F_{SC} \quad [2]$$

where $F_{TE} = \langle [\overline{v'm'}] \rangle$ and $F_{SC} = \langle [\overline{v}\ \overline{m}] \rangle$ are the MSE flux by transient eddies and stationary circulation (mean meridional circulation plus stationary eddies), respectively, $\nabla \cdot F_{TOA} = TOA$ and $\nabla \cdot F_{SFC} = SFC$ are in flux form where TOA and SFC are the TOA radiative and surface energy fluxes with the global mean removed, $\langle \cdot \rangle$ denotes a mass-weighted vertical integration, $[\cdot]$ denotes a zonal average, $\bar{\cdot}$ denotes a monthly average, i.e. an average over a particular month not the climatological monthly average, and $'$ denotes a deviation from the monthly average (12). The removal of the global mean emphasizes meridional gradients (15, 43).

An equation for extratropical storminess in each hemisphere is obtained by integrating equation (2) between 20° and the pole:

$$\underbrace{\widehat{F_{TE}}}_{STM} = \underbrace{\widehat{F_{TOA}}}_{TOA} - \underbrace{\widehat{F_{SFC}}}_{SFC} - \underbrace{\widehat{F_{SC}}}_{SC}. \quad [3]$$

where $\widehat{(\cdot)} = \int_{90°}^{20°} 2\pi \cos\phi(\cdot) d\phi$. For the climatology, the SC contribution to the storminess asymmetry is dominated by stationary eddies. The energetic storminess asymmetry is defined as

$$(-\widehat{F_{TE,SH}} - \widehat{F_{TE,NH}})/\widehat{F_{TE,NH}} \quad [4]$$

to account for southward energy flux in the Southern Hemisphere. The MSE budget of the hemispheric asymmetry in ECHAM6 is closed to within 5%. More specifically, the hemispheric asymmetry of atmospheric energy flux calculated using TOA radiative and surface energy fluxes differs from the hemispheric asymmetry of atmospheric energy flux calculated using the 6 hourly wind and MSE data by 5%. For the observations, the SFC term is inferred as a residual (see above) and for the CMIP5 simulations the SC term is inferred as a residual because the coarse vertical pressure grid makes the computation of SC inaccurate.

The energetic storminess is significantly correlated with eddy kinetic energy across the model simulations and reanalysis data ($R^2 = 0.98$, Fig. S10) consistent with previous work (12, 44–46). The latent energy flux contribution accounts for energetic storminess being larger in SYMS than FLAT in Fig. 2f even though eddy kinetic energy is larger in FLAT than SYMS (Fig. S11). Note the larger latent energy flux in SYMS does not affect our overall conclusion that topography and ocean circulation contribute roughly equally to the storminess asymmetry because the role of each can only be attributed to within the nonlinearity, which is 3% (Fig. 2e, F+S), or the accuracy of closing of the MSE budget, which is 5%.

In order to quantitatively compare the hemispheric asymmetry of eddy kinetic energy to energetic storminess we rescale energetic storminess following previous work (45, 46). A rescaling factor of $\widehat{EKE_{SH}}/\widehat{F_{TE,SH}} = -0.29$ is applied to the Southern Hemisphere and $\widehat{EKE_{NH}}/\widehat{F_{TE,NH}} = 0.33$ to the Northern Hemisphere, which leads to a rescaling of 0.65 for the storminess asymmetry. Note that a similar rescaling approach is used when connecting eddy kinetic energy to mean available potential energy (11).

ACKNOWLEDGMENTS. T.A.S., O.M. and A.D. acknowledge support from NSF (AGS-1742944, AGS-2033467 and AGS-2019647).

1. Y Guo, EKM Chang, SS Leroy, How strong are the Southern Hemisphere storm tracks? *Geophys. Res. Lett.* **36**, 10.1029/2009GL040733 (2009).
2. BJ Hoskins, KI Hodges, New perspectives on the Northern Hemisphere winter storm tracks. *J. Atmos. Sci.* **59**, 1041–1061 (2002).
3. BJ Hoskins, KI Hodges, A new perspective on Southern Hemisphere storm tracks. *J. Clim.* **18**, 4108–4129 (2005).
4. TA Shaw, et al., Storm track processes and the opposing influences of climate change. *Nat. Geosc.* **9**, 10.1038/NGEO2783 (2016).
5. DL Hartmann, *Global Physical Climatology*. (Elsevier), p. 453 (2016).
6. S Pfhal, H Wernli, Quantifying the relevance of cyclones for precipitation extremes. *J. Clim.* **25**, 6770–6780 (2012).
7. M Messmer, I Simmonds, Global analysis of cyclone-induced compound precipitation and wind extreme events. *Weather. Clim. Extrem.* p. 10.1016/j.wace.2021.100324 (2021).
8. S Bony, et al., Clouds, circulation and climate sensitivity. *Nat. Geosc.* **8**, 10.1038/NGEO2398 (2015).
9. S Manabe, TB Terpstra, The effect of mountains on the general circulation of the atmosphere as identified by numerical experiments. *J. Atmos. Sci.* **31**, 3–42 (1974).
10. PA O'Gorman, Understanding the varied response of the extratropical storm tracks to climate change. *Proc. Nat. Acad. Sci.* **107**, 10.1073/pnas.1011547107 (2010).
11. PA O'Gorman, T Schneider, Energy of midlatitude transient eddies in idealized simulations of changed climates. *J. Clim.* **21**, 5797–5806 (2008).
12. TA Shaw, P Barpanda, A Donohoe, A moist static energy framework for zonal-mean storm-track intensity. *J. Atmos. Sci.* **75**, 1979–1994 (2018).
13. H Wang, M Ting, Seasonal cycle of the climatological stationary waves in the NCEP–NCAR reanalysis. *J. Atmos. Sci.* **56**, 3892–3919 (1999).
14. IM Held, M Ting, H Wang, Northern winter stationary waves: Theory and modeling. *J. Clim.* **15**, 2125–2144 (2002).
15. A Donohoe, DS Battisti, What determines meridional heat transport in climate models? *J. Clim.* **25**, 3832–3850 (2012).
16. DMWF Frierson, et al., Contribution of ocean overturning circulation to tropical rainfall peak in the Northern Hemisphere. *Nat. Geos.* **6**, 10.1038/NGEO1987 (2013).
17. GL Stephens, et al., The curious nature of the hemispheric symmetry of the Earth's water and energy balances. *Curr. Clim. Chang. Rep.* **2**, 135–147 (2016).
18. GK Vallis, *Climate and the oceans*. (Princeton University Press), p. 231 (2012).
19. R Seager, et al., Is the gulf stream responsible for Europe's mild winters? *Quart. J. Roy. Soc.* **128**, 2563–2586 (2002).
20. DJ Brayshaw, T Woollings, M Velllinga, Tropical and extratropical responses of the North Atlantic atmospheric circulation to a sustained weakening of the MOC. *J. Clim.* **22**, 3146–3155 (2009).
21. C Wilson, B Sinha, RG Williams, The effect of ocean dynamics and orography on atmospheric storm tracks. *J. Clim.* **22**, 3689–3702 (2009).
22. Y Kaspi, T Schneider, Winter cold of eastern continental boundaries induced by warm ocean waters. *Nature* **471**, 10.1038/nature09924 (2011).
23. T Woollings, JM Gregory, JG Pinto, M Reyers, DJ Brayshaw, Response of the North Atlantic storm track to climate change shaped by ocean-atmosphere coupling. *Nat. Geos.* **5**, 10.1038/NGEO1438 (2012).
24. KC Armour, J Marshall, JR Scott, A Donohoe, ER Newsom, Southern Ocean warming delayed by circumpolar upwelling and equatorward transport. *Nat. Geosc.* **9**, 10.1038/NGEO2731 (2016).
25. DL Hartmann, P Ceppi, Trends in the CERES dataset, 2000–13: The effects of sea ice and jet shifts and comparison to climate models. *J. Clim.* **27**, 2444–2456 (2014).
26. C Derksen, R Brown, Spring snow cover extent reductions in the 2008–2012 period exceeding climate model projections. *Geophys. Res. Lett.* p. 10.1029/2012GL053387 (2012).
27. RJ Stouffer, S Manabe, K Bryan, Interhemispheric asymmetry in climate response to a gradual increase of atmospheric CO2. *Nature* **342**, 660–662 (1989).
28. S Manabe, RJ Stouffer, MJ Spelman, K Bryan, Transient responses of a coupled ocean-atmosphere model to gradual changes of atmospheric CO2. Part I: Annual mean response. *J. Clim.* **4**, 785–818 (1991).
29. LC Hahn, KC Armour, MD Zelinka, CM Bitz, A Donohoe, Contributions to polar amplification in CMIP5 and CMIP6 models. *Front. Earth Sci.* **9**, 10.3389/feart.2021.710036 (2021).
30. R Chemke, LM Polvani, Opposite tropical circulation trends in climate models and in reanalyses. *Nat. Geosc.* **17**, 10.1038/s41561–019–0383–x (2019).
31. EA Barnes, JA Screen, The impact of Arctic warming on the midlatitude jet-stream: Can it? Has it? Will it? *WIREs Clim. Chang.* **6**, 10.1002/wcc.337 (2015).
32. RJ Stouffer, et al., The role of continental topography in the present-day ocean's mean climate. *J. Clim.* pp. 10.1175/JCLID–20–0690.1 (2021).
33. NMJ Hall, B Dong, PJ Valdes, Atmospheric equilibrium, instability and energy transport at the Last Glacial Maximum. *Clim. Dyn.* **12**, 497–511 (1996).
34. C Li, DS Battisti, Reduced Atlantic storminess during Last Glacial Maximum: Evidence from a coupled climate model. *J. Clim.* **21**, 3561–3579 (2008).
35. A Donohoe, DS Battisti, Causes of reduced North Atlantic storm activity in a CAM3 simulation of the Last Glacial Maximum: Theory and modeling. *J. Clim.* **22**, 4793–4808 (2009).
36. A Donohoe, KC Armour, GS Roe, DS Battisti, The partitioning of atmospheric energy transport and changes under climate forcing in coupled climate models. *J. Clim.* **33**, 4141–4165 (2020).
37. A Donohoe, DS Battisti, The seasonal cycle of atmospheric heating and temperature. *J. Clim.* **26**, 4962–4980 (2013).
38. KE Trenberth, JT Fasullo, An observational estimate of ocean energy divergence. *J. Phys. Ocean.* **38**, 985–999 (2008).
39. M Wild, et al., The global energy balance from a surface perspective. *Clim. Dyn.* **40**, 3107–3134 (2013).
40. M Wild, et al., The energy balance over land and oceans: An assessment based on direct observations and cmip5 climate models. *Clim. Dyn.* **44**, 3393–3429 (2015).
41. R Chemke, LM Polvani, Linking midlatitudes eddy heat flux trends and polar amplification. *npj Clim. Atmos. Sci.* **8**, 10.1038/s41612–020–0111–7 (2020).
42. B Stevens, et al., Atmospheric component of the MPI-M Earth System Model: ECHAM6. *J. Adv. Model. Earth Syst.* **5**, 146–172 (2013).
43. SM Kang, IM Held, DMWF Frierson, M Zhao, The response of the ITCZ to extratropical thermal forcing: Idealized slab-ocean experiments with a GCM. *J. Clim.* **21**, 3521–3532 (2008).
44. P Barpanda, TA Shaw, Surface fluxes modulate the seasonality of zonal-mean storm tracks. *J. Atmos. Sci.* **77**, 753–779 (2020).
45. TA Shaw, RJ Graham, Hydrological cycle changes explain weak Snowball Earth storm track despite increased surface baroclinicity. *Geophys. Res. Lett.* p. 10.1029/2020GL089866 (2020).
46. TA Shaw, Z Smith, The midlatitude response to polar sea ice loss: Idealized slab-ocean aquaplanet experiments with thermodynamic sea ice. *J. Clim.* **35**, 2633–2649 (2022).